Chapter 3

Mutation of a Highly Conserved Pore-Lining Leucine Residue Increases Agonist Sensitivity of GluCl

Abstract

The glutamate-gated chloride channel (GluCl) is an invertebrate, ligand-gated anion channel of the Cys-loop receptor family. It is activated by the endogenous neurotransmitter glutamate and by the antiparasitic drug ivermectin (IVM). A crystal structure of the *Caenorhabditis elegans* GluCl α homopentamer shows the location of the glutamate binding site, the separate ivermectin binding site, and the highly conserved leucine residue at the 9' position of the pore-lining M2 transmembrane domain. Mutation of this L9' residue in other Cys-loop receptors dramatically increases agonist sensitivity. Using whole-cell patch clamp, we found that six of seven mutations (L9'S, A, F, I, T, V, but not G) at this position in the α subunit increased the glutamate sensitivity of the heteromeric GluCl αβ channel by factors of 5- to 90-fold. Beta-branched amino acids (Ile, Thr, Val) gave the greatest reductions in EC_{50}. Analysis of side chain properties revealed that helix-destabilizing energy correlated with increased glutamate sensitivity. Many L9' mutations also increased background conductance, suggesting a higher probability of unliganded openings. Only one mutation, L9'F, resulted in increased glutamate sensitivity without increasing spontaneous activity. A fluorescent membrane potential assay confirmed that the L9'F mutation also increased IVM sensitivity. In addition, it was determined that GluCl α homomers indeed form functional, IVM-sensitive channels in mammalian systems. However, GluCl α homomers bearing a L9'F mutation do not show increased sensitivity to IVM, implying incorporation of the β subunit is necessary for the gain-of-function effect. Increasing GluCl sensitivity to ivermectin will benefit its use as a neuronal silencing tool.

Introduction

Ion channel receptors of the Cys-loop superfamily are known to mediate fast-synaptic transmission in vertebrate and invertebrate nervous systems. Vertebrate receptors include the nicotinic acetylcholine (nAChR), serotonin (5-HT_3R), γ-aminobutyric acid type A and C ($GABA_{A/C}$R), glycine (GlyR), and zinc-activated (ZAC) receptors. Invertebrate receptors include a variation of channels gated by these same neurotransmitters in addition to others gated by glutamate (GluCl), histamine (HisCl), tyramine (LGC-55), and pH (pHCl, SsCl). Each class of receptors is comprised of a variety of species-specific subunits, capable of forming receptor subtypes with different functional properties. Each individual Cys-loop receptor is a pentameric complex, with five subunits symmetrically arranged around a central ion-conducting pore. Receptor subtypes are typically heteromeric, however subunits of some receptor classes can form functional and physiologically relevant homomers. All subunits share a common topology composed of a large N-terminal extracellular domain, four helical transmembrane domains (M1–M4), and a variable intracellular loop (M3–M4 loop). The helical M2 domain of each subunit lines the channel pore. Activation of Cys-loop receptors by their respective neurotransmitter gates the entry and/or exit of specific ions through this pore, resulting in a change in membrane potential.

The glutamate-gated chloride (GluCl) channel is an invertebrate Cys-loop receptor with a distinct pharmacological profile. GluCl chloride currents are gated by the traditional neurotransmitter glutamate and the semi-synthetic anthelmintic drug ivermectin (IVM). A 3.3-Å-resolution crystal structure of a modified homomeric GluCl channel reveals the binding site locations for each of these agonists (Figure 3-1A, B)[1].

Glutamate binds at the classical neurotransmitter binding site located in the extracellular domain at the interface of two subunits. Ivermectin binds at a separate, unconventional site, inserting at the upper periphery of the transmembrane helices also at the interface of two adjacent subunits. Structural coordinates of the channel represent an open-pore conformation with the side-chains of pore-lining residues clearly defined (Figure 3-1C, D). One pore-lining residue, leucine 9' (L9'), resides in the middle of the M2 transmembrane domain. L9' is highly conserved among subunits of the Cys-loop receptor family and has been proposed to serve as a hydrophobic channel gate (Figure 3-1E, F)[2-4].

Many studies using various Cys-loop receptors have shown that mutation of L9' to one of several other residues can dramatically increase agonist sensitivity, apparent by a leftward shift in the dose-response curve, allowing channel activation with lower concentrations of agonist[5-13]. Increases in agonist sensitivity have been attributed to effects on channel gating resulting in longer open channel dwell times[5,6,10,11,14]. Other 9' mutational effects have also been described including slowed apparent desensitization[5-8,11,12] and increased spontaneous activity. Spontaneous activity has been indicated by both a large resting conductance that is sensitive to open pore blockers[9,12,14-17] as well as single channel events observed in the absence of agonist[5,14,17]. L9' mutations may also render some partial agonists as full agonists[18] or even convert an antagonist into an agonist[19]. In contrast, some L9' mutant studies have shown no increase in agonist sensitivity[8,16,20,21], no increase in spontaneous activity[16,20], or no blockade of a large resting conductance with specific channel blockers[21] for a selection of L9' mutations. These inconsistencies could be due, in part, to the assortment of amino acids substituted into the L9' position. For example, it has been consistently reported that polarity of the amino acid mutation

influences the gain in agonist sensitivity for several cationic receptors, with more polar amino acids showing a greater reduction in EC_{50} for the muscle type nAChRs[10,11], neuronal α7 nAChRs[7], and 5-HT_3Rs[8]. Aside from this, no other correlations between the functional behavior displayed by L9' mutant receptors, (e.g., cationic versus anionic, heteromeric versus homomeric) and the identity of the amino acid substitution have been determined.

The current study investigates the effect of seven different L9' mutations in the *Caenorhabditis elegans* GluCl receptor. Mutational effects are examined by assaying electrophysiological responses in the presence and absence of agonist as well as changes in membrane potential using a voltage-sensitive fluorescent dye. The L9' gain-of-function effect has been examined exclusively using traditional neurotransmitter agonists. It is unclear whether an L9' mutation would enable a similar increase in sensitivity for an agonist activating the channel at a different binding site location on the receptor, such as IVM. An L9' mutation that allows GluCl to be activated by a lower concentration of IVM would be beneficial toward the application of GluCl/IVM as an electrical silencing tool in mammalian neuronal circuitry studies[22,23].

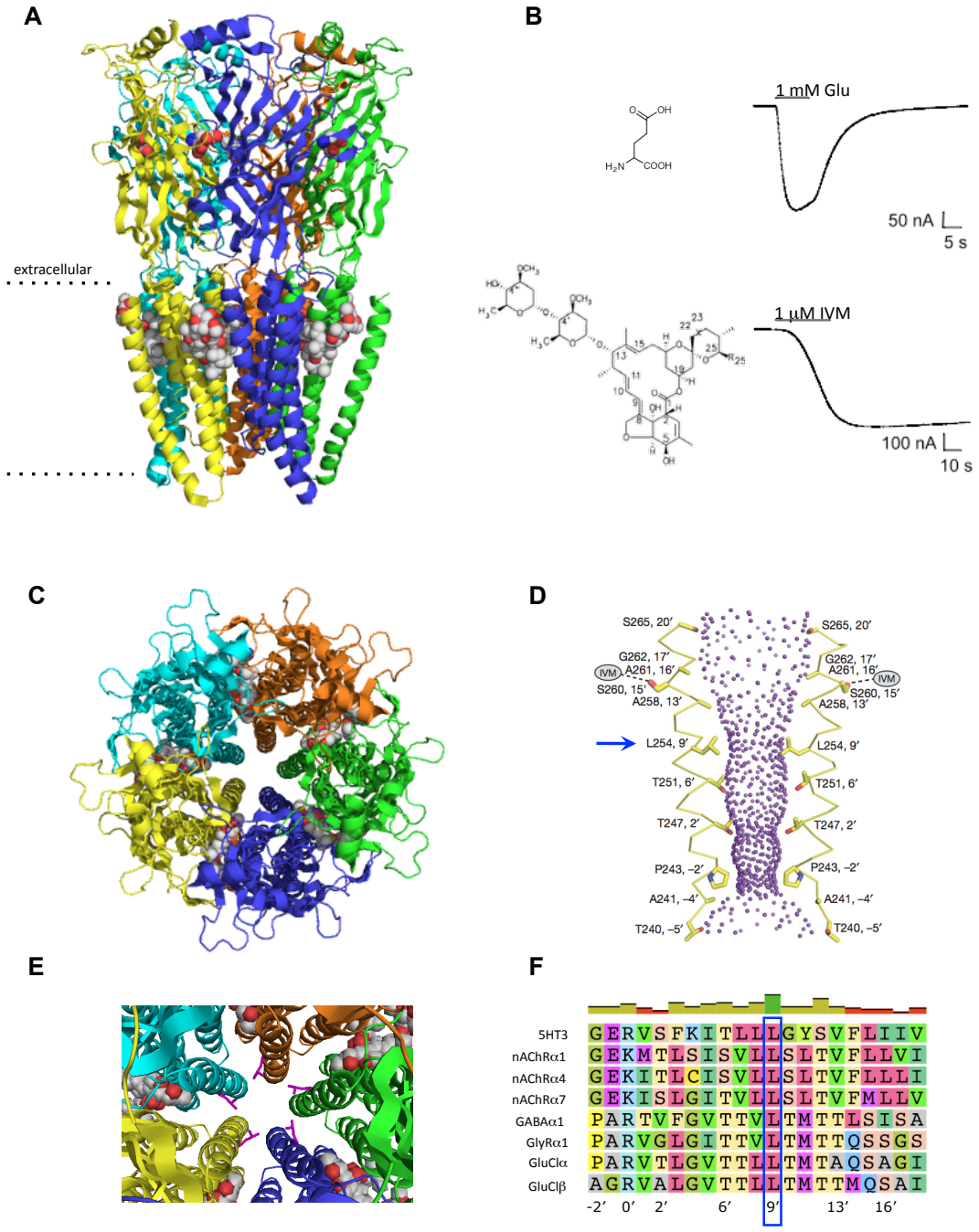

Figure 3-1. The GluCl channel. *A.* Crystal structure (side view) of a modified GluCl α homomeric channel with glutamate and IVM molecules bound (3RIF.pdb). Agonists bind at subunit interfaces; glutamate binds in the extracellular domain, IVM binds at the top half of the transmembrane domain. *B.* GluCl is differentially activated by glutamate and IVM. Electrophysiological traces were obtained from heteromeric GluCl αβ channels expressed in *Xenopus* oocytes (figure adapted from Li et al., 2002[24]). *C.* Top view of the GluCl channel showing symmetrical arrangement of subunits forming the pore. *D, E, & F.* Residues of the helical pore-lining M2 domain. Leucine 9' is a highly conserved pore-lining residue. (Figure *D.* adapted from Hibbs & Gouaux, 2011.)[1]

Results

L9' mutations increase glutamate sensitivity

The highly conserved leucine 9' residue in the M2 domain of the α subunit was mutated to each of seven other residues, L9'I, F, V, A, G, S, T. The heteromeric GluCl αβ wild-type (WT), fluorescently tagged (WT-XFP), and L9' mutant channels (also -XFP tagged) were expressed in HEK293 cells and examined for glutamate sensitivity using the millisecond microperfusion capability of the Dynaflow Pro II chip. Whole-cell concentration-response relations were obtained. Each patched cell was exposed to at least seven glutamate concentrations applied in increasing order. One-second glutamate applications induced fast-activating current responses followed by complete ligand washout upon bath solution postapplication (Figure 3-2A). Currents were activated in a concentration-dependent manner. Normalized concentration-response curves and Hill fit parameters are shown in Figure 3-2B and Table 3-1. A saturating dose was unable to be applied in some cases, as pre-exposure of glutamate, which accumulates in the cell reservoir from the lanes of laminar flow over time, appeared to desensitize receptors leading to reduced or undetected current responses. Response normalization to a less-than-saturating concentration, as is the case for the WT and L9'G mutant receptors, leads to an overestimation of glutamate sensitivity (i.e., a lower, inaccurate estimation of EC_{50}). All other L9' mutations significantly increased glutamate sensitivity by a factor of 5- to 90-fold, as determined by EC_{50}, compared to the WT-XFP receptor (Figures 3-2C; Table 3-1). Maximum current responses for the L9' mutant channels, however, were significantly reduced (Figure 3-2D). In addition, many cells expressing L9' mutant channels revealed a large holding current prior to application of glutamate, which was

often predictable by a lack of capacitive transients in whole-cell configuration. Such observations are characteristic of membrane leakiness, presuming the cells maintained seal resistance and were not sick or dead. Leak currents are likely due to an increased probability of unliganded channel openings resulting from the L9' mutation.

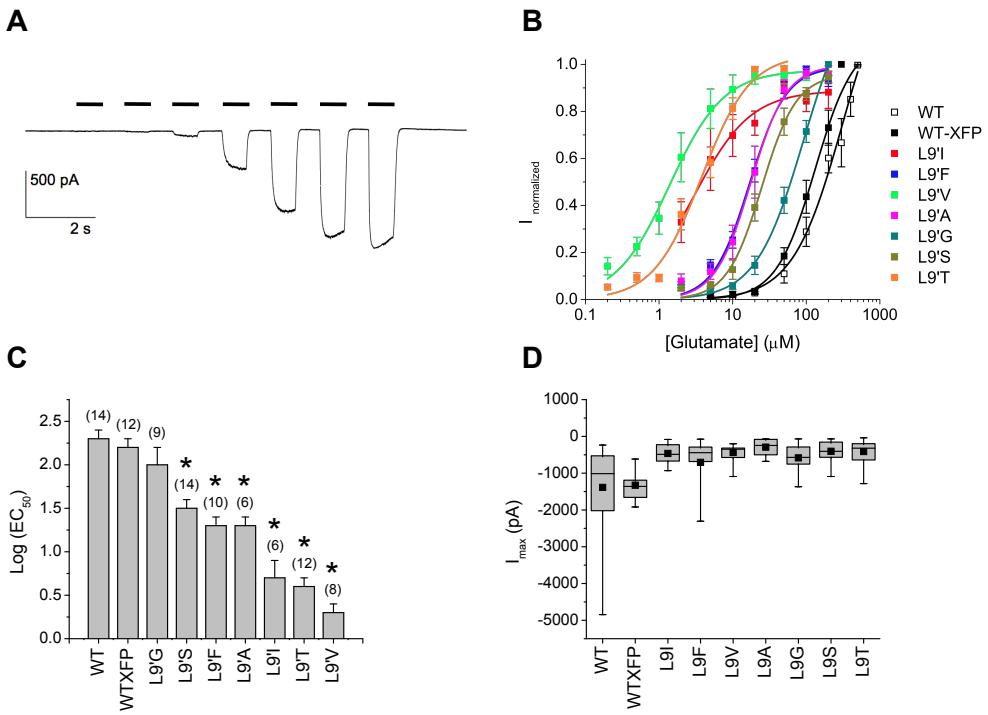

Figure 3-2. Glutamate activation of heteromeric GluCl αβ wild-type (WT), fluorescently tagged (WT-XFP), and L9' mutant channels. *A.* Whole-cell patch clamp recording of glutamate-induced current from the WT receptor expressed in HEK293 cells. Black bars indicate 1-second applications of 5, 10, 20, 50, 100, 200, and 500 μM glutamate. *B.* Glutamate concentration-response curves fit with the Hill equation. *C.* All 9' mutant channels except L9'G significantly increased glutamate sensitivity. *D.* Maximum induced current (I_{max}) from glutamate activation. Current magnitudes are represented as negative values.

GluCl channel	abbr.	EC_{50} (μM)	Hill	n
α(WT) + β(WT)	WT	314 ± 133*	1.28 ± 0.23	14
α-YFP + β-CFP	WT-XFP	132 ± 5	1.64 ± 0.07	12
β(WT) homomer		NR		
α-YFP L9'V homomer		NR		
α-YFP L9'I + β-CFP	L9'I	3.0 ± 0.4	1.13 ± 0.23	6
α-YFP L9'F + β-CFP	L9'F	17.0 ± 1.8	1.75 ± 0.27	10
α-YFP L9'V + β-CFP	L9'V	1.4 ± 0.1	1.18 ± 0.11	8
α-YFP L9'A + β-CFP	L9'A	17.7 ± 1.6	1.79 ± 0.24	6
α-YFP L9'G + β-CFP	L9'G	91.8 ± 17.1*	1.34 ± 0.14	9
α-YFP L9'S + β-CFP	L9'S	24.9 ± 1.7	1.84 ± 0.17	14
α-YFP L9'T + β-CFP	L9'T	3.8 ± 0.6	1.32 ± 0.18	12

Table 3-1. Glutamate activation parameters of GluCl WT, WT-XFP, and L9' mutant channels. Parameters correspond to concentration-response curves in Figure 3-2B. The EC_{50} and Hill coefficient values represent the mean ± SEM for the number of cells (n) recorded. The * indicates response normalization to a less-than-saturating maximum concentration.

Functional studies of GluCl receptors expressed in *Xenopus laevis* oocytes using two-electrode voltage clamp have demonstrated that homomeric channels of both α and β subunits are functional, but they exhibit contrasting agonist activation profiles. Homomeric GluCl α channels are activated directly by IVM, but not glutamate, while homomeric GluCl β channels are activated directly by glutamate, but not IVM[25]. It has since been determined that α homomers do in fact maintain glutamate binding sites, but are deficient in coupling glutamate binding events to channel gating[1,26]. In the present study, no glutamate-induced currents were recorded from HEK293 cells transfected with GluCl β(WT) cDNA only, probably because homomeric GluCl β channels are not expressed at the plasma membrane. Discrepancies in surface expression between mammalian systems and oocytes have been observed for other membrane proteins and are assumed to be the result of different protein trafficking mechanisms[27-30]. The

possibility that presence of an L9' mutation now allowed GluCl α homomers to be gated by glutamate was also considered. No currents were recorded from the L9'V α homomer for the glutamate concentrations applied (≤ 500 μM).

Whole-cell glutamate concentration-response relations for a given receptor were subject to a great deal of cell-to-cell variability. Different cells recorded on the same day, from the same culture dish, using the same glutamate solutions, displayed very different concentration-dependent responses, even for the WT receptor (Figure 3-3A). Desensitization kinetics also varied greatly from cell-to-cell. To examine this variability, concentration-response curves for individual cells were compared. Individual response curves could be separated into distinct categories based on sensitivity (Figure 3-3B, Table 3-2). This wide range in agonist sensitivity was evident with all L9' mutants except for L9'F (Figure 3-3C, Table 3-2). Typically, heteromeric receptor expression that gives rise to multiple agonist sensitivities is due to the presence of different stoichiometric populations which result in biphasic concentration-response relations[31-33]. It is assumed that an individual cell would express some fraction of each receptor stoichiometry. Interestingly, for GluCl, most individual cells display a monophasic concentration-response relationship. It is unclear whether the various glutamate sensitivities are due to stoichiometric preferences or some other inherent inconsistencies (e.g., cross-contamination, phenotypic diversity) within HEK293 cell cultures[34,35].

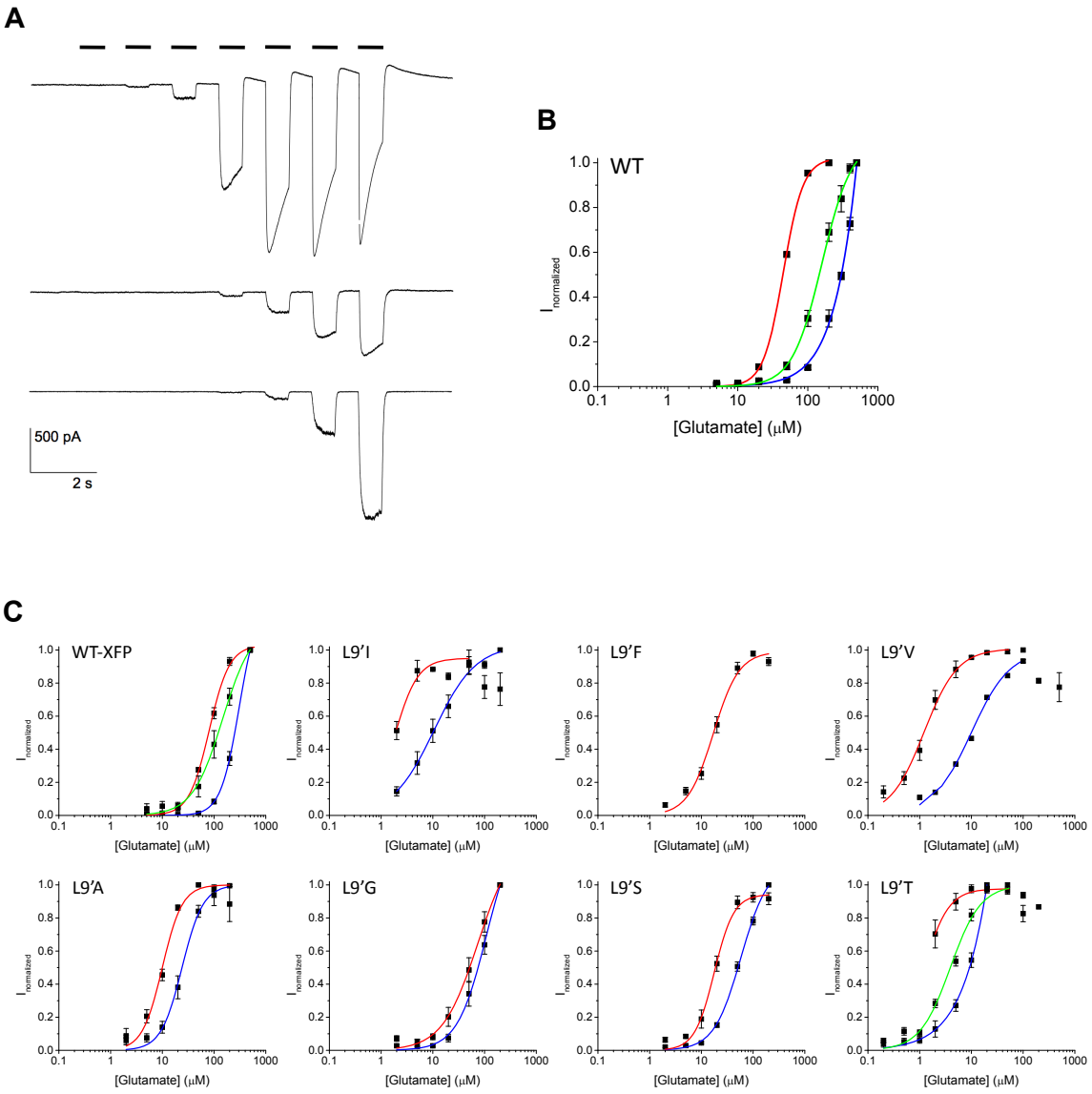

Figure 3-3. Cell-to-cell variability of glutamate concentration-response relations. *A.* Cells expressing GluCl WT receptor recorded on the same day, from the same culture dish, responded differently to application of the same glutamate solutions (see Figure 3-2 for concentrations). *B.* Concentration response curves of individual cells could be separated into three categories: high sensitivity (red line), low sensitivity (blue line), and mixed (green line). *C.* Cell-to-cell variability was observed for nearly all mutant receptors tested.

	High Sensitivity			Mixed			Low Sensitivity		
	EC_{50} (μM)	Hill	n	EC_{50} (μM)	Hill	n	EC_{50} (μM)	Hill	n
WT	44.71 ± 0.00	3.05 ± 0.17	1	159.65 ± 0.01	2.03 ± 0.12	9	2564.9 ± 3.98*	1.45 ± 0.15	4
WT-XFP	80.68 ± 0.00	2.22 ± 0.13	6	145.91 ± 0.02	1.49 ± 0.16	3	306.90 ± 0.01*	2.41 ± 0.09	3
αL9'I	1.80 ± 0.00*	1.91 ± 0.67	3				10.57 ± 0.00	1.08 ± 0.12	3
αL9'F	17.25 ± 0.00	1.75 ± 0.17	10						
αL9'V	1.22 ± 0.00	1.34 ± 0.15	7				9.95 ± 0.00	1.17 ± 0.11	1
αL9'A	9.99 ± 0.00	2.25 ± 0.30	4				24.04 ± 0.00	2.13 ± 0.25	2
αL9'G	74.14 ± 0.02	1.26 ± 0.16	5				108.86 ± 0.02*	1.54 ± 0.16	4
αL9'S	17.76 ± 0.00	2.29 ± 0.34	9				58.13 ± 0.00	1.67 ± 0.11	5
αL9'T	1.19 ± 0.00*	1.81 ± 0.39	3	3.91 ± 0.00	1.48 ± 0.16	7	500.12 ± 2.48*	0.92 ± 0.11	2

Table 3-2. Variability in glutamate activation parameters for heteromeric GluCl αβ WT, WT-XFP, and L9' mutant channels. Parameters correspond to concentration-response curves in Figure 3-3B, C. The EC_{50} and Hill coefficient values represent the mean ± SEM for the number of cells (n) recorded. The * indicates response normalization to a less-than-saturating maximum concentration.

L9' mutational effect on EC_{50} correlates with alpha-helical destabilization

Studies involving the cation-selective Cys-loop receptors suggest the magnitude of increased agonist sensitivity was influenced by the polarity of the L9' mutation[8,10,11]. To check for a correlation between the identity of the amino acid mutation and the magnitude of increased agonist sensitivity, the log(EC_{50}) value of each L9' mutant channel was plotted against several physical properties of the amino acid side-chain, including hydrophobicity[36], surface area[37], and propensity towards α-helix stabilization[38]. GluCl L9' mutations show no functional relationship dependent on side-chain hydrophobicity or side-chain surface area (Figure 3-4A, B). A potential trend in surface area is negated by the fact that Leu and Ile have nearly the same surface area (180 $Å^2$ vs. 182 $Å^2$) but give very different EC_{50} values. There does appear to be a correlation between the identity of the L9' mutant side-chain and its effect on α-helix stabilization (Figure 3-4C). Excluding the two extremes of Ala, the amino acid with the highest helical

propensity[39,40], and Gly, which is given a value of zero on most scales as it lacks a contributing side-chain, the energy values associated with disrupting the stability of the pore-lining α-helix do trend with the shifts in EC_{50}. The less stable the helix (higher energy), the more sensitive the receptor is to glutamate (lower EC_{50}). The three β-branched amino acids, Ile, Val, and Thr, give the largest gain-of-function shifts in EC_{50} for the L9' mutant channels. β-branched amino acids are known to destabilize an α-helix due to a loss of side chain conformational entropy[41-43]. Specifically, the rotational freedom of a β-branched side-chain is restricted by steric hindrance, in that substituents in a γ-position of the side chain interfere with the carbonyl oxygen atoms of the residues *i* – 2 and *i* – 3 in the helix. Overall, destabilization of the M2 pore-lining α-helix at the L9' position may lower the energy barrier for the closed-to-open conformational change making it easier for the channel to open in the presence of agonist.

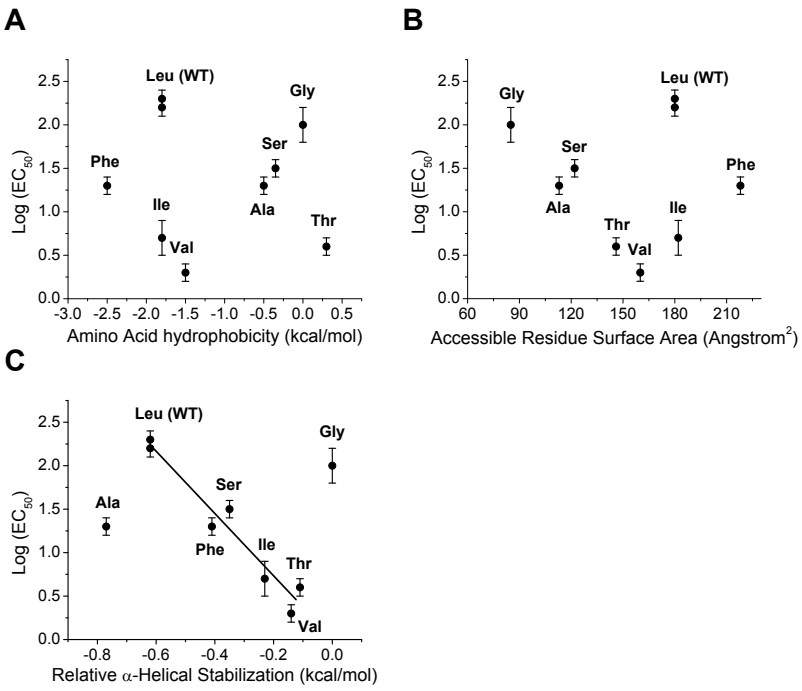

Figure 3-4. Functional relationships of L9' mutant channels with physical properties of amino acid mutation. *A & B.* The L9' gain-of-function effect is not dependent on side-chain hydrophobicity or side-chain surface area. *C.* The L9' gain-of-function effect does correlate with side-chain disruption of an α-helical conformation. Ala and Gly residues are considered outliers. Line represents a linear regression fit of the seven other data points. Two data points for Leu represent those for the WT and WT-XFP receptors.

L9' mutations increase background conductance

Destabilization of the pore-lining helix may also be responsible for the large holding currents and lack of whole-cell transients observed prior to glutamate application. A more flexible gate could increase the probability of spontaneous channel openings which would contribute to the background conductance of a cell at rest. The presence of spontaneous channel activity is often confirmed by the use of open-channel blockers in the absence of agonist. Picrotoxin and fipronil sulfone are known pore blockers of GluCl[44,45]. However, they have both been reported to exhibit differential blocking effects

on the desensitizing and nondesensitizing components of glutamate evoked currents, presumably due to differences in subunit stoichiometry[46-49]. It has also been demonstrated in several studies that the typical blocking mechanism of picrotoxin is impaired with both agonist activated and spontaneously open receptors bearing L9' mutations[9,16,21]. Therefore, the use of pore blockers is not practical for assaying the amount of background conductance for the various GluCl L9' mutant channels. Instead, a voltage ramp protocol was adopted[50].

Cells were voltage clamped in whole-cell configuration with no capacitive compensation. The voltage was ramped continuously from −60 mV to +60 mV over 50 ms in the absence of ligand. An example of a WT current response is shown in Figure 3-5A. The background conductance was measured from the slope of the resistive current ramp and normalized by the mean membrane capacitance of each receptor, which could be calculated from the capacitive current offset. Because it can be difficult to distinguish between cells with a leaky membrane and patches with a poor seal, cells with a seal resistance less than 40 MΩ, corresponding to a chord conductance of > 25 nS, were omitted. GluCl WT and WT-XFP receptors show minimal background conductance that is not different from a mock-transfected control (Figure 3-5B). The two L9' mutations with the smallest side-chains, L9'A and L9'G, had the largest background conductance which was significantly different from WT receptors. Notably, these are the same two L9' mutants that were not in accordance with the disruption of α-helical stability correlation. The three L9' mutants with β-branched side-chains did have a greater background conductance than WT receptors on average, but the increase was not statistically significant for the number of cells sampled.

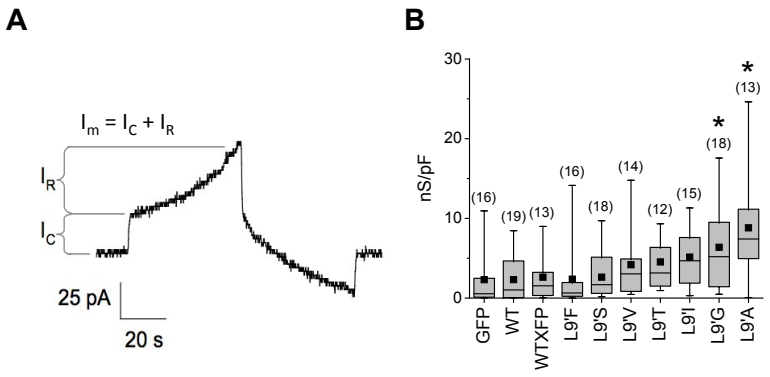

Figure 3-5. Background conductance of GluCl receptors in absence of ligand. *A*. Example of a current response from GluCl WT. Whole-cell voltage-clamped cells with no capacitive compensation were ramped from −60 mV to +60 mV over 50 ms. The total current across the membrane I_m is the sum of the capacitive current I_c, and the resistive current, I_R. *B.* Background conductance normalized by the mean capacitance of each receptor for the number of cells recorded (shown in parentheses). Soluble GFP was used as a mock-transfection control.

The L9' gain-of-function effect is maintained for IVM

It was unknown whether an L9' mutation would maintain a gain-of-function gating effect for an agonist that activates the channel through a different allosteric mechanism (e.g., IVM) than that triggered by a typical neurotransmitter binding event (e.g., glutamate). Assaying channel function with IVM by electrophysiology, however, is challenging. IVM is a lipophilic compound with limited ligand washout, making it difficult to apply successive doses to an individual cell which is necessary for concentration-response normalization. To circumvent this, L9' mutant receptor activation was measured by a fluorescence-based assay using a membrane potential-sensitive dye.

Glutamate activation and IVM activation were first measured individually for GluCl WT channels. Even with this indirect functional assay, different response kinetics

were apparent for the two agonists, resembling the differences observed in their direct electrophysiological response[25]. Specifically, the raw signal (in relative fluorescence units, RFU) induced by glutamate reaches a maximum within 3 min, followed by a decline for nonsaturating concentrations. The IVM-induced signal is slower to rise but remains at maximum for up to 5 min (Figure 3-6A). Both glutamate and IVM generated fluorescent signals for GluCl WT and WT-XFP receptors in a concentration-dependent manner (Figure 3-6B). All L9' mutants, except for L9'F, displayed a much weaker signal for both glutamate and IVM activation (Figure 3-6C). The reduced signal results from elevated baseline fluorescence (Figure 3-6D) which is likely a reflection of the increased background conductance observed for these mutants. Normalization of the raw RFU signal indicates that the L9'F mutation increases receptor sensitivity to both glutamate and IVM compared to WT and WT-XFP receptors (Figure 3-6E). Glutamate activation parameters are comparable to those obtained by electrophysiology (Table 3-3). IVM activation parameters reveal that WT-XFP receptors do not have the same concentration-dependent relationship as WT receptors, and the L9'F mutant receptor displays a biphasic concentration-dependent response.

Homomeric channels were assayed once more for agonist activation using the membrane potential dye. As expected, GluCl α(WT) homomers were not activated by glutamate. GluCl α(WT) homomers were, however, responsive to IVM (Figure 3-7). This was unexpected as previous studies report that no current was obtained from mammalian cells when the α subunit was expressed alone[23,51]. GluCl α-XFP homomers, as well as those containing the L9'F mutation were also responsive, producing much steeper and right-shifted concentration-response curves for IVM (Table 3-4). Removal of the XFP tag

from the L9'F mutant channel did not recover IVM sensitivity. This implies two things: (1) that the XFP insertion is having some functional effect on GluCl activation by IVM that was not apparent with glutamate, and (2) that incorporation of the β subunit is necessary for the increased IVM sensitivity observed with the heteromeric GluCl L9'F mutant. GluCl β(WT) homomers did not respond to glutamate or IVM applications.

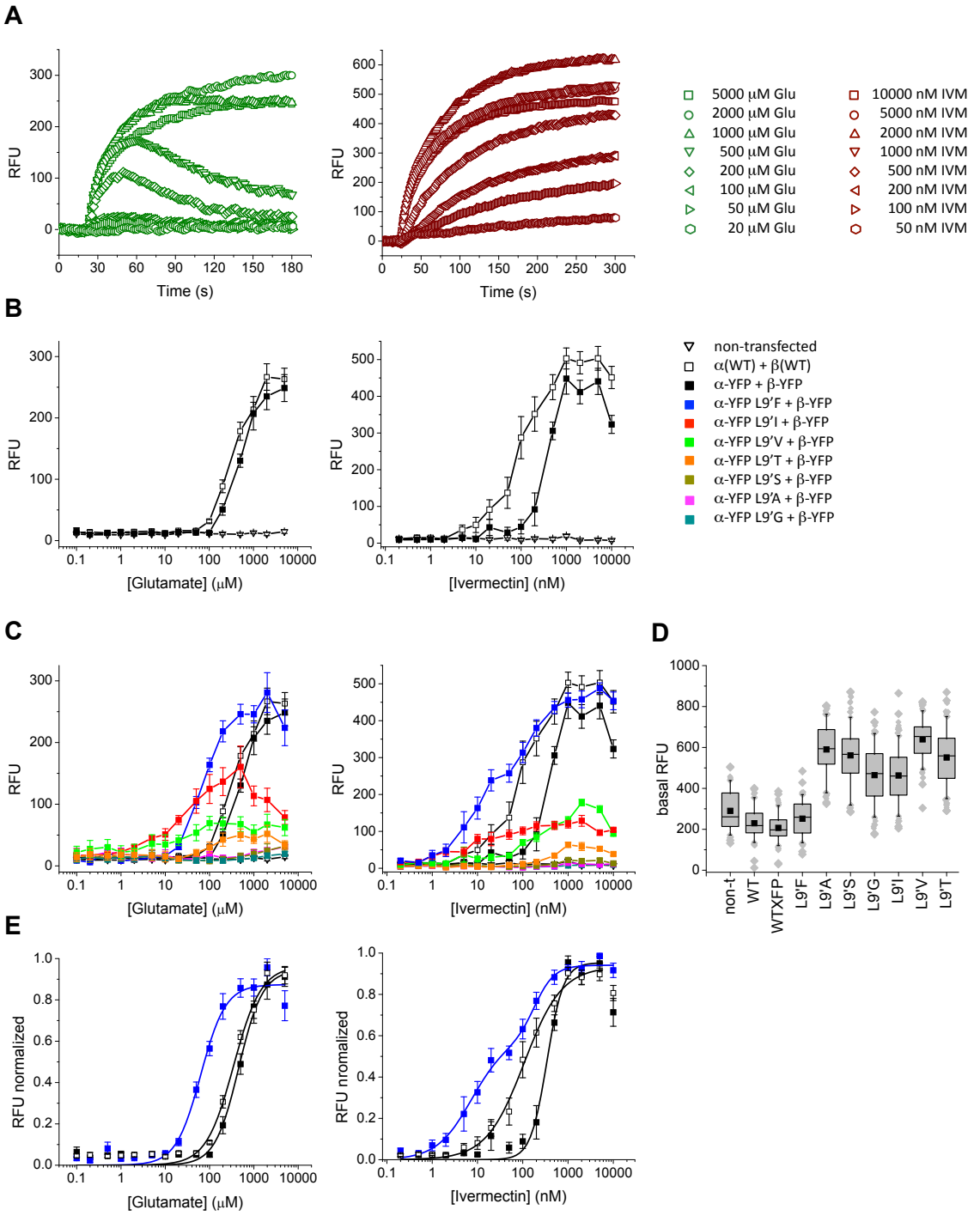

Figure 3-6. Heteromeric GluCl αβ WT, WT-XFP, and L9' mutant receptor activation measured by a fluorescent membrane potential-sensitive dye. *(Left panel: glutamate activation; Right panel: IVM activation) A*. Example of raw RFU signal for GluCl WT (8 of 15 responses shown). *B.* RFU signals for GluCl WT and WT-XFP are concentration-dependent. Nontransfected cells do not respond to agonist. *C & D.* All L9' mutants receptors, except for L9'F, show diminished agonist-induced RFU signals and elevated baseline RFU signals. *E.* Normalized concentration-response curves for GluCl WT, WT-XFP, and L9'F mutant receptors. The concentration-response relation for IVM activation of the L9'F mutant was best fit by the sum of two Hill equations.

	Glu activation		*IVM activation*	
GluCl channel	**EC_{50} (μM)**	**Hill**	**EC_{50} (nM)**	**Hill**
α(WT) + β(WT)	349.00 ± 44.29	1.40 ± 0.18	138.45 ± 9.60	1.04 ± 0.06
α-YFP + β-YFP	455.80 ± 53.14	1.62 ± 0.23	342.64 ± 31.52	2.41 ± 0.39
α-YFP L9'F + β-YFP	63.07 ± 7.12	1.55 ± 0.24	7.27 ± 2.85 *(61%)*	1.14 ± 0.24
			185.35 ± 50.16	1.99 ± 0.82

Table 3-3. Activation parameters acquired with the membrane potential assay for heteromeric GluCl αβ WT, WT-XFP, and L9'F mutant channels. Parameters correspond to concentration-response curves in Figure 3-6E. The EC_{50} and Hill coefficient values represent the mean ± SEM for six measurements. The high sensitivity component of the biphasic L9'F curve corresponds to 61% of the normalized response.

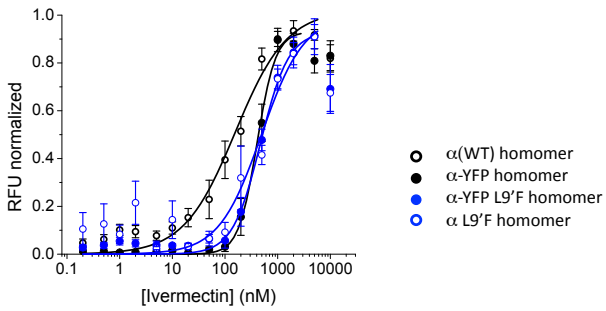

Figure 3-7. Ivermectin activation of homomeric GluCl α WT, WT-XFP, and L9'F mutant channels. Normalized concentration-response curves were fit with the Hill equation.

	IVM activation	
GluCl channel	**EC_{50} (nM)**	**Hill**
α(WT) homomer	285.51 ± 75.17	1.01 ± 0.15
α-YFP homomer	406.88 ± 21.08	2.47 ± 0.24
α-YFP L9'F homomer	472.67 ± 44.23	1.64 ± 0.19
α L9'F homomer	492.99 ± 95.91	1.07 ± 0.20

Table 3-4. Ivermectin activation parameters for homomeric GluCl α WT, WT-XFP, and L9'F mutant channels. Parameters correspond to concentration-response curves in Figure 3-7. The EC_{50} and Hill coefficient values represent the mean ± SEM for six measurements.

Discussion

L9' effects

Mutational effects of L9' have varied across the family of Cys-loop receptors and are dependent on the physical properties of the amino acid being introduced. Even the slightest differences are likely to have big functional consequences in such a critical region of the channel. For GluCl, six of seven L9' mutations significantly increased glutamate sensitivity, and not all of the L9' mutants show increased spontaneous activity. This is the first report of a correlation between pore-lining helix stability and agonist sensitivity. According to the Monod-Wyman-Changeux (MWC) model of allosteric activation[52], channel gating (i.e., events that enable the closed-to-open state transitions) involves global conformational changes within and across subunits. Destabilization of the M2 α-helix by β-branched amino acids may lower the energy barrier for a closed-to-open conformational change making it easier for the channel to open both in the presence (apparent from the left-shifted EC_{50}) and absence (apparent from the increased background conductance) of agonist. However, the L9'A mutant, which should form the most stable pore-lining helix, actually shows the greatest increase in background conductance. It may be that the 9' position requires a large, hydrophobic, non-β-branched side-chain to stabilize the closed state conformation. Whether or not the L9' residue prevents ion flow by physically occluding the channel pore cannot be determined from this study.

Variability from cell-to-cell during the electrophysiology experiments made it difficult to draw conclusions about any L9' mutational effects on receptor desensitization.

In general, it appeared that high sensitivity glutamate responses for all receptors showed more desensitization. This may also be reflected in the raw glutamate-induced signals of the membrane potential assays (Figure 3-6A, left panel). For example, signal responses for low concentrations, which would activate high sensitivity channels, show a decline after the first minute of glutamate application. As higher concentrations are applied low sensitivity channels, which do not desensitize, would become activated so the signal no longer declines over time.

Stoichiometry

There is some evidence for the co-existence of two pharmacologically distinct and physiologically relevant GluCl channels. Invertebrate neuron recordings display glutamate-induced currents comprised of variable fractions of desensitizing and non-desensitizing components, which were blocked differentially by picrotoxin and fipronil sulfone[46-49]. These differential pore-blocking effects may be explained by a subunit specific dependence of blockade[44], suggesting the presence of more than one GluCl stoichiometry.

The biphasic IVM concentration-response curve of the L9'F mutant in the membrane potential assay supports a mixed stoichiometry hypothesis. The glutamate concentration-response relation obtained for this mutant, however, is monophasic. Furthermore, the L9'F mutant was the only receptor that did not show variation in glutamate sensitivity during whole-cell patch-camp recordings. It is possible the 10 cells patched were not representative of the entire transiently transfected cell population.

While patch-clamp experiments directly sample individual cells, sample sets are small and can be biased by cell selection and sealing success of the experimenter. The membrane potential assay, on the other hand, is a population measurement. Any cell-to-cell variability is coalesced into a single composite response.

With expression of GluCl in HEK293 cells, glutamate activated currents are most likely conducted by heteromeric receptors, since β homomers are probably not expressed at the cell surface and α homomers are not directly gated by glutamate. It is conceivable that different receptor stoichiometries do not differ significantly in glutamate sensitivity, resulting in a concentration-dependence that is uninterrupted. The biphasic heteromeric and monophasic homomeric concentration-response curves for the L9'F mutant indicate that incorporation of the β subunit significantly increases IVM sensitivity. The precise stoichiometric ratio of α:β subunits cannot be determined from this functional study. It should also be noted that the number of bound IVM molecules required to gate the channel is unknown. It cannot be ruled out that the number of agonists bound could influence the biphasic concentration response.

Studies employing L9' mutations in all five subunits have shown that the extent of increased agonist sensitivity was dependent on the number of subunits containing L9' substitutions, i.e., the magnitude of EC_{50} shifts were additive[5,6,9,53]. It was consequently inferred that each subunit provides independent and equivalent contributions to channel gating. More detailed analysis of this mutagenesis data found that L9' effects of individual subunits are not identical, rather, the various subunits bearing L9' mutations contribute unequally to channel gating[10,14,18,20,53]. The gain-of-function effect of an L9' mutation appears to be influenced by the structurally asymmetric pore of a heteromeric

channel compared to the perfectly symmetrical pore geometry of homomers. The influence of asymmetry is especially apparent in the present study, as heteromeric channels bear L9' mutations only in the α subunit; the β subunit still contains Leu at this position. A ring of five L9'F mutations as in the α homomer does not increase sensitivity to IVM. Differences in constitutive activity between heteromeric and homomeric receptors have also been reported[20].

FlexStation assay limitations

In the membrane potential assay, the voltage sensitive dye partitions across the cell membrane depending on the resting membrane potential of the cell. Dye quenchers are present in the extracellular solution. Upon stimulus, the dye follows movement of positively charged ions, so membrane depolarization allows the dye to enter the cell where it is dequenched resulting in a positive fluorescent signal. Conversely, during hyperpolarization, dye is requenched as it exits the cell resulting in a negative fluorescent signal. The positive fluorescent signal observed in the present study following induction of Cl^- currents therefore seems counterintuitive. A similar result, however, has been observed and eloquently discussed for HEK293 cells expressing GlyR[54]. In short, as an embryonic cell line, HEK293 cells have a relatively high intracellular chloride concentration compared to other mammalian cells, so channel opening allows efflux, rather than influx, of Cl^- current thereby decreasing the separation of charge and resulting in depolarization of the membrane. Elevated basal levels of fluorescence and negligible agonist-induced responses were observed in a related GlyR study with receptors

containing other M2 domain mutations[55]. The authors propose constitutive activation as a possible explanation. The present study confirms that receptors with increased levels of spontaneous activity do show elevated basal signals and diminished responses to agonist application in a membrane potential assay. An increased background conductance likely affects distribution of the dye during the incubation period. The amount of de-quenched dye that has already entered the cell is high, so the amount of additional dye moving into the cell upon application of agonist is low. Since the assay only measures changes in membrane potential rather than inherent values, a diminished signal is observed.

L9'F as an optimized silencer

We have previously demonstrated that an engineered GluCl channel can be used to selectively silence electrical activity in targeted CNS neurons *in vivo* when activated by IVM. Both α and β subunits were necessary in order to achieve silencing. GluCl α homomers were reportedly not expressed. This study shows that α homomers are indeed expressed and that α-XFP homomers require greater concentrations of IVM for activation. Introduction of an L9'F mutation may promote β subunit incorporation as a method of increasing IVM sensitivity. Unlike other mutants, L9'F substantially increased agonist sensitivity without increasing background conductance, a fundamental requirement as spontaneous openings would be detrimental to the goal of a pharmacologically induced silencer. While all L9' mutants reduced the maximum glutamate response of patch-clamped cells, the fluorescent signal generated by L9'F mutants in the membrane potential assay was not diminished compared to WT receptors.

Nevertheless, HEK293 cells generally produce massive currents, so it is conceivable that the L9'F mutant receptor would conduct sufficient Cl^- current to silence a neuron. Altogether, introduction of an L9'F mutation may enhance the GluCl/IVM silencing tool.

Materials and Methods

Site-Directed Mutagenesis

Previously described plasmid vector pcDNA3.1/V5-His TOPO (Invitrogen #K4800-01) containing the complete optimized coding sequence for either unlabeled or fluorescently tagged *Caenorhabditis elegans* GluCl α and β subunits, namely optGluCl αWT, optGluCl βWT, optGluCl α-YFP, and optGluCl β-YFP[56], were used in this study. Note, 'opt' has been removed from the nomenclature in this text. Enhanced yellow fluorescent protein (YFP) insertions are located within the intracellular M3-M4 loop[24]. Leucine 9' mutations were made using the QuikChange II XL site-directed mutagenesis kit (Agilent Technologies #200522) with PfuTurbo DNA polymerase (Agilent Technologies #600250) using the following forward and reverse primers: 5' – CC CTG GGC GTG ACC ACC CTG xxx AC – 3' and 5' – GC GGA CTG AGC GGT CAT GGT xxx CA – 3', where 'xxx' delineates the mutated Leu9' codon. Leu9' mutations included Ile, Phe, Val, Ser, Thr, Ala, and Gly. All mutations were confirmed by DNA sequencing.

Cell Culture

Human embryonic kidney (HEK) 293 cells were purchased from ATCC (#CRL-1573). Cells were cultured in Dulbecco's modified Eagle's medium (DMEM; Gibco #11965) supplemented with 10% FBS (Gibco #26140), 100 units/ml penicillin, 100 μg/ml streptomycin (Gibco #15140), and 1 mM sodium pyruvate (Gibco #11360), and maintained at 37°C and 5% CO_2 in a humidified incubator. Cells were passaged when

confluent at a subcultivation ratio of 1:5 or 1:10 every 3 to 4 days. For electrophysiology experiments, HEK293 cells were plated at a density of 150,000 cells/dish in 35 mm culture dishes. GluCl receptors were expressed via transient transfection for which 1 µg DNA in 100 µl DMEM was combined with 4 µl ExpressFect (Denville Scientific #E2650) in 100 µl DMEM that was pre-incubated for 20 minutes before adding to culture dishes containing 2 ml fresh culture medium. For FlexStation assays, HEK293 cells were plated at 20,000 cells/well, with a plating volume of 100 µl/well, in a black-sided/clear-bottomed 96-well imaging plate (BD Falcon #353219). For transfection, 16 µg total DNA in 750 µl DMEM was mixed with 30 µl ExpressFect in 750 µl DMEM, pre-incubated for 20 minutes, and then added at 15 µl/well to cells containing 100 µl fresh culture media. For both electrophysiology and FlexStation assays, cells were transfected 24 hours after plating and assayed 48 hours after transfection. Transfection mixes were removed from cultures following a 4–6 hour incubation period at 37°C/5% CO_2 and replaced with fresh culture medium.

Electrophysiology

Whole-cell patch-clamp recordings were obtained using an Axopatch 200A amplifier with a CV201 headstage and Digidata 1200 series interface (Axon Instruments). A Hum Bug device (Quest Scientific) was used to eliminate 50/60 Hz noise. Data was acquired using Clampex 9.2 software (Axon Instruments). Dose-response data was recorded at a sampling frequency of 5 kHz with lowpass filtering at 1 kHz in Gap-free acquisition mode. Voltage ramp data was sampled at 10 kHz with lowpass filtering at 5 kHz in

Episodic Stimulation acquisition mode. External bath recording solution contained (in mM): 140 NaCl, 2.8 KCl, 2 $CaCl_2$, 2 $MgCl_2$, 10 D-glucose, 10 HEPES, 5 NaOH, pH 7.35, 330 mOsm. Internal patch pipette solution contained (in mM): 130 CsCl, 4 $MgCl_2$, 4 Na_2-ATP, 1 EGTA, 10 HEPES, 10 CsOH, pH 7.35, 315 mOsm. Pipettes were made from borosilicate glass with resistances of 4–10 MΩ. Co-transfection of soluble pmaxGFP (Amaxa) was used to identify transfected HEK293 cells. Cells were voltage-clamped with a holding potential of −60 mV. All recordings were performed at ambient temperature.

Glutamate concentration-response experiments were conducted using the Dynaflow Pro II system, a millisecond microperfusion chip (Cellectricon). GluCl-expressing HEK293 cells initially plated in 35 mm plastic culture dishes were washed with bath solution, detached using a cell scraper, and declumped by trituration to produce a 500 µl volume of round cells in suspension. Cells were added 100 µl at a time to 2 ml fresh bath solution intermittently to avoid lengthy pre-exposure to glutamate due to accumulation from the lanes of laminar flow into the cell reservoir. Na^+ glutamate (Sigma #G1626) was dissolved in water as a 100 mM stock and stored as 1 ml aliquots at -20°C. Glutamate concentrations, prepared as serial dilutions in bath solution, were applied in increasing order for 1 second each, alternating with 1 second applications of external bath solution for complete ligand washout.

A continuous voltage ramp protocol was used to measure background conductance in the absence of ligand. Cells were whole-cell voltage-clamped at −60 mV with no capacitive compensation then ramped from −60 mV to +60 mV over 50 ms.

Membrane Potential Measurements

A fluorescence-based assay employing the FLIPR Membrane Potential Assay Kit, BLUE formulation, (Molecular Devices, #R8042) was used to detect voltage changes across the cell membrane. The dye reagent is of proprietary composition[57]. Dye loading buffer was prepared according to package literature. Specifically, the contents of one vial of BLUE reagent was dissolved with 5 ml of 1x Assay Buffer, followed by a wash of the vial with another 5 ml of 1x Assay Buffer, to yield a total volume of 10 ml of dye loading buffer. Unused portions of dye loading buffer were stored at -20°C and used within 5 days. For the functional assay, culture medium was removed from the cells and replaced with 50 µl DMEM. Cells were then loaded with 50 µl of Blue dye loading buffer and incubated for 40 min at 37°C/5% CO_2. The signal was detected using the FlexStation 3 multimode benchtop microplate reader operated by SoftMax Pro Data Acquisition & Analysis Software (Molecular Devices). Excitation and emission wavelengths were set at 530 nm and 565 nm, respectively, with an emission cut-off of 550 nm. Plate reads were performed at ambient temperature with a 'Low PMT' setting. Run times, of which the first 20 s measured basal fluorescence, were 180 s for glutamate-induced signals or 300 s for ivermectin-induced signals. Other FlexStation parameters included a pipette height of 230 µl, an initial well volume of 100 µl, a transfer volume of 50 µl (therefore, drug concentrations were prepared 3x), and a transfer rate setting of 2, corresponding to ~31 µl/sec. Glutamate concentrations were prepared from 100 mM aliquots as 1:10 serial dilutions of 5, 2, and 1 mM dissolved in a 1x commercial stock of Hanks' balanced salt solution (HBSS, without phenol red; Invitrogen #14025) with 20 mM HEPES, pre-adjusted to pH 7.4 with sodium hydroxide. Ivermectin (Sigma #18898) was dissolved in

DMSO as a 10 mM stock and stored as 0.3 mM aliquots at -20°C. Ivermectin concentrations for the FlexStation assay were prepared as 1:10 serial dilutions of 10, 5, and 2 μM using 1x HBSS with 20 mM HEPES at pH 7.4, containing 0.1% DMSO.

Data Analysis

Electrophysiology data was analyzed using Clampfit 9.2 software. Glutamate-induced currents were normalized for each cell individually by the maximal current response for that cell. Concentration-response curves were constructed and fit to the following sigmoid Hill function in Origin 7.0 (OriginLab),

$$y = V_{max}\left(\frac{x^n}{k^n + x^n}\right)$$

which can be rewritten as,

$$\frac{I}{I_{max}} = \frac{1}{1 + \left(\frac{EC_{50}}{[A]}\right)^H}$$

where I is the amount of current induced by a given agonist concentration [A], I_{max} is the maximum current induced, EC_{50} is the concentration required to elicit half the maximal response and H is the Hill coefficient.

For voltage ramp experiments, the total current, I_m, can be broken down as the sum of the capacitive current, I_C, and the resistive current, I_R, across the membrane ($I_m = I_C + I_R$). Background conductance, G, was measured from the slope of the resistive current ramp ($G = dI_R/dV$). Membrane capacitance, C_m, was calculated by measuring the

capacitive current from the offset of the current ramp ($I_C = C_m(dV/dt)$). The background conductance was then normalized by the mean capacitance for each receptor and plotted as mean ± SEM from 12 or more cells. To distinguish a large background conductance from poor sealing of the patch pipette, cells with a seal resistance of < 40 MΩ, corresponding to a chord conductance of > 25 nS (as determined by G = I/V = 1/R), were omitted.

Raw FlexStation signals were exported as '.txt' files from SoftMax Pro 5 and analyzed offline using Microsoft Excel 2008 and Origin 7.0. Relative fluorescent unit signals were zeroed by mean subtraction of the first 5 data points, then smoothed using a 3-point sliding average before determining the maximum data point per well. Six, 15-point concentration-response data sets were obtained from a single 96-well plate, set up as 2 columns of 8 wells including a blank, repeated 5 more times in subsequent columns. Signals of each well were normalized by the maximum signal for that particular 2-column set to compensate for signal run-down over time. Normalized data was then averaged to construct concentration-response curves as described above.

Statistics

Pooled data for each mutation are shown as means ± SEM. Boxplots represent the mean, median, 25^{th}, and 75^{th} percentiles. Statistical significance ($P < 0.05$) was determined by one-way analysis of variance (ANOVA) on ranks using multiple pairwise comparison.

Acknowledgments

Thanks to Herwig Just and Sindhuja Kadambi for point mutation and sequencing primers.

References

1. Hibbs RE, Gouaux E. (2011) Principles of activation and permeation in an anion-selective Cys-loop receptor. *Nature* **474**:54–60.

2. Unwin N. (1993) Nicotinic acetylcholine receptor at 9 Å resolution. *J Mol Biol* **229**:1101–1124.

3. Miyazawa A, Fujiyoshi Y, Unwin N. (2003) Structure and gating mechanism of the acetylcholine receptor pore. *Nature* **423**:949–955.

4. Beckstein O, Sansom MS. (2006) A hydrophobic gate in an ion channel: the closed state of the nicotinic acetylcholine receptor. *Phys Biol* **3**:147–159.

5. Labarca C, Nowak MW, Zhang H, Tang L, Deshpande P, Lester HA. (1995) Channel gating governed symmetrically by conserved leucine residues in the M2 domain of nicotinic receptors. *Nature* **376**:514–516.

6. Filatov GN, White MM. (1995) The role of conserved leucines in the M2 domain of the acetylcholine receptor in channel gating. *Mol Pharmacol* **48**:379–384.

7. Revah F, Bertrand D, Galzi JL, Devillers-Thiery A, Mulle C, Hussy N, Bertrand S, Ballivet M, Changeux JP. (1991) Mutations in the channel domain alter desensitization of a neuronal nicotinic receptor. *Nature* **353**:846–849.

8. Yakel JL, Lagrutta A, Adelman JP, North RA. (1993) Single amino acid substitution affects desensitization of the 5-hydroxytryptamine type 3 receptor expressed in Xenopus oocytes. *Proc Natl Acad Sci U S A* **90**:5030–5033.

9. Chang Y, Weiss DS. (1999) Allosteric activation mechanism of the α1β2γ2 gamma-aminobutyric acid type A receptor revealed by mutation of the conserved M2 leucine. *Biophys J* **77**:2542–2551.

10. Kearney PC, Zhang H, Zhong W, Dougherty DA, Lester HA. (1996) Determinants of nicotinic receptor gating in natural and unnatural side chain structures at the M2 9' position. *Neuron* **17**:1221–1229.

11. Kosolapov AV, Filatov GN, White MM. (2000) Acetylcholine receptor gating is influenced by the polarity of amino acids at position 9' in the M2 domain. *J Membr Biol* **174**:191–197.

12. Thompson SA, Smith MZ, Wingrove PB, Whiting PJ, Wafford KA. (1999) Mutation at the putative GABA(A) ion-channel gate reveals changes in allosteric modulation. *Br J Pharmacol* **127**:1349–1358.

13. Shan Q, Nevin ST, Haddrill JL, Lynch JW. (2003) Asymmetric contribution of α and β subunits to the activation of αβ heteromeric glycine receptors. *J Neurochem* **86**:498–507.

14. Bianchi MT, Macdonald RL. (2001) Mutation of the 9' leucine in the GABA(A) receptor γ2L subunit produces an apparent decrease in desensitization by stabilizing open states without altering desensitized states. *Neuropharmacology* **41**:737–744.

15. Bertrand S, Devillers-Thiery A, Palma E, Buisson B, Edelstein SJ, Corringer PJ, Changeux JP, Bertrand D. (1997) Paradoxical allosteric effects of competitive inhibitors on neuronal α7 nicotinic receptor mutants. *Neuroreport* **8**:3591–3596.

16. Chang Y, Weiss DS. (1998) Substitutions of the highly conserved M2 leucine create spontaneously opening ρ1 gamma-aminobutyric acid receptors. *Mol Pharmacol* **53**:511–523.

17. Pan ZH, Zhang D, Zhang X, Lipton SA. (1997) Agonist-induced closure of constitutively open gamma-aminobutyric acid channels with mutated M2 domains. *Proc Natl Acad Sci U S A* **94**:6490–6495.

18. Gleitsman KR, Shanata JA, Frazier SJ, Lester HA, Dougherty DA. (2009) Long-range coupling in an allosteric receptor revealed by mutant cycle analysis. *Biophys J* **96**:3168–3178.

19. Bertrand D, Devillers-Thiery A, Revah F, Galzi JL, Hussy N, Mulle C, Bertrand S, Ballivet M, Changeux JP. (1992) Unconventional pharmacology of a neuronal nicotinic receptor mutated in the channel domain. *Proc Natl Acad Sci U S A* **89**:1261–1265.

20. Dalziel JE, Cox GB, Gage PW, Birnir B. (2000) Mutating the highly conserved second membrane-spanning region 9' leucine residue in the α(1) or β(1) subunit produces subunit-specific changes in the function of human α(1)β(1) gamma-aminobutyric Acid(A) receptors. *Mol Pharmacol* **57**:875–882.

21. Tierney ML, Birnir B, Pillai NP, Clements JD, Howitt SM, Cox GB, Gage PW. (1996) Effects of mutating leucine to threonine in the M2 segment of α1 and β1 subunits of GABAA α1β1 receptors. *J Membr Biol* **154**:11–21.

22. Haubensak W, Kunwar PS, Cai H, Ciocchi S, Wall NR, Ponnusamy R, Biag J, Dong HW, Deisseroth K, Callaway EM, Fanselow MS, Luthi A, Anderson DJ. (2010) Genetic dissection of an amygdala microcircuit that gates conditioned fear. *Nature* **468**:270–276.

23. Lerchner W, Xiao C, Nashmi R, Slimko EM, van Trigt L, Lester HA, Anderson DJ. (2007) Reversible silencing of neuronal excitability in behaving mice by a genetically targeted, ivermectin-gated Cl- channel. *Neuron* **54**:35–49.

24. Li P, Slimko EM, Lester HA. (2002) Selective elimination of glutamate activation and introduction of fluorescent proteins into a Caenorhabditis elegans chloride channel. *FEBS Lett* **528**:77–82.

25. Cully DF, Vassilatis DK, Liu KK, Paress PS, Van der Ploeg LH, Schaeffer JM, Arena JP. (1994) Cloning of an avermectin-sensitive glutamate-gated chloride channel from Caenorhabditis elegans. *Nature* **371**:707–711.

26. Etter A, Cully DF, Schaeffer JM, Liu KK, Arena JP. (1996) An amino acid substitution in the pore region of a glutamate-gated chloride channel enables the coupling of ligand binding to channel gating. *J Biol Chem* **271**:16035–16039.

27. Leduc-Nadeau A, Lussier Y, Arthus MF, Lonergan M, Martinez-Aguayo A, Riveira-Munoz E, Devuyst O, Bissonnette P, Bichet DG. (2010) New autosomal recessive mutations in aquaporin-2 causing nephrogenic diabetes insipidus through deficient targeting display normal expression in Xenopus oocytes. *J Physiol* **588**:2205–2218.

28. Moeller HB, Fenton RA. (2010) Can one Bad Egg' really spoil the batch? *J Physiol* **588**:2283–2284.

29. Smit LS, Strong TV, Wilkinson DJ, Macek M, Jr., Mansoura MK, Wood DL, Cole JL, Cutting GR, Cohn JA, Dawson DC, et al. (1995) Missense mutation (G480C) in the CFTR gene associated with protein mislocalization but normal chloride channel activity. *Hum Mol Genet* **4**:269–273.

30. Yasui M, Hazama A, Kwon TH, Nielsen S, Guggino WB, Agre P. (1999) Rapid gating and anion permeability of an intracellular aquaporin. *Nature* **402**:184–187.

31. Moroni M, Bermudez I. (2006) Stoichiometry and pharmacology of two human α4β2 nicotinic receptor types. *J Mol Neurosci* **30**:95–96.

32. Nelson ME, Kuryatov A, Choi CH, Zhou Y, Lindstrom J. (2003) Alternate stoichiometries of α4β2 nicotinic acetylcholine receptors. *Mol Pharmacol* **63**:332–341.

33. Zhou Y, Nelson ME, Kuryatov A, Choi C, Cooper J, Lindstrom J. (2003) Human α4β2 acetylcholine receptors formed from linked subunits. *J Neurosci* **23**:9004–9015.

34. ATCC. Cell line authentication test recommendations. in *ATCC: Technical Bulletin No. 8* (2007).

35. Nakamura N, Yamazawa T, Okubo Y, Iino M. (2009) Temporal switching and cell-to-cell variability in Ca2+ release activity in mammalian cells. *Mol Syst Biol* **5**:247.

36. Eisenberg D, Weiss RM, Terwilliger TC. (1984) The hydrophobic moment detects periodicity in protein hydrophobicity. *Proc Natl Acad Sci U S A* **81**:140–144.

37. Miller S, Janin J, Lesk AM, Chothia C. (1987) Interior and surface of monomeric proteins. *J Mol Biol* **196**:641–656.

38. O'Neil KT, DeGrado WF. (1990) A thermodynamic scale for the helix-forming tendencies of the commonly occurring amino acids. *Science* **250**:646–651.

39. Marqusee S, Robbins VH, Baldwin RL. (1989) Unusually stable helix formation in short alanine-based peptides. *Proc Natl Acad Sci U S A* **86**:5286–5290.

40. Pace CN, Scholtz JM. (1998) A helix propensity scale based on experimental studies of peptides and proteins. *Biophys J* **75**:422–427.

41. Creamer TP, Rose GD. (1992) Side-chain entropy opposes alpha-helix formation but rationalizes experimentally determined helix-forming propensities. *Proc Natl Acad Sci U S A* **89**:5937–5941.

42. Dao-Pin S, Baase WA, Matthews BW. (1990) A mutant T4 lysozyme (Val 131→Ala) designed to increase thermostability by the reduction of strain within an alpha-helix. *Proteins* **7**:198–204.

43. Hermans J, Anderson AG, Yun RH. (1992) Differential helix propensity of small apolar side chains studied by molecular dynamics simulations. *Biochemistry* **31**:5646–5653.

44. Etter A, Cully DF, Liu KK, Reiss B, Vassilatis DK, Schaeffer JM, Arena JP. (1999) Picrotoxin blockade of invertebrate glutamate-gated chloride channels: subunit dependence and evidence for binding within the pore. *J Neurochem* **72**:318–326.

45. Ikeda T, Zhao X, Kono Y, Yeh JZ, Narahashi T. (2003) Fipronil modulation of glutamate-induced chloride currents in cockroach thoracic ganglion neurons. *Neurotoxicology* **24**:807–815.

46. Raymond V, Sattelle DB, Lapied B. (2000) Co-existence in DUM neurones of two GluCl channels that differ in their picrotoxin sensitivity. *Neuroreport* **11**:2695–2701.

47. Zhao X, Salgado VL, Yeh JZ, Narahashi T. (2004) Kinetic and pharmacological characterization of desensitizing and non-desensitizing glutamate-gated chloride channels in cockroach neurons. *Neurotoxicology* **25**:967–980.

48. Zhao X, Yeh JZ, Salgado VL, Narahashi T. (2004) Fipronil is a potent open channel blocker of glutamate-activated chloride channels in cockroach neurons. *J Pharmacol Exp Ther* **310**:192–201.

49. Zhao X, Yeh JZ, Salgado VL, Narahashi T. (2005) Sulfone metabolite of fipronil blocks gamma-aminobutyric acid- and glutamate-activated chloride channels in mammalian and insect neurons. *J Pharmacol Exp Ther* **314**:363–373.

50. Schmitt BM, Koepsell H. (2002) An improved method for real-time monitoring of membrane capacitance in Xenopus laevis oocytes. *Biophys J* **82**:1345–1357.

51. Slimko EM, McKinney S, Anderson DJ, Davidson N, Lester HA. (2002) Selective electrical silencing of mammalian neurons in vitro by the use of invertebrate ligand-gated chloride channels. *J Neurosci* **22**:7373–7379.

52. Monod J, Wyman J, Changeux JP. (1965) On the Nature of Allosteric Transitions: A Plausible Model. *J Mol Biol* **12**:88–118.

53. Chang Y, Wang R, Barot S, Weiss DS. (1996) Stoichiometry of a recombinant GABAA receptor. *J Neurosci* **16**:5415–5424.

54. Jensen AA, Kristiansen U. (2004) Functional characterisation of the human α1 glycine receptor in a fluorescence-based membrane potential assay. *Biochem Pharmacol* **67**:1789–1799.

55. Jensen AA, Bergmann ML, Sander T, Balle T. (2010) Ginkgolide X is a potent antagonist of anionic Cys-loop receptors with a unique selectivity profile at glycine receptors. *J Biol Chem* **285**:10141–10153.

56. Slimko EM, Lester HA. (2003) Codon optimization of Caenorhabditis elegans GluCl ion channel genes for mammalian cells dramatically improves expression levels. *J Neurosci Methods* **124**:75–81.

57. Krahn T, Paffhausen W, Schade A, Bechem M, Schmidt D. (2002) US Patent 6,420,183. *Chem Abstr* **128**:59162.